



# Green synthesis of ZnO nanoparticles from ball moss (*Tillandsia recurvata*) extracts: characterization and evaluation of their photocatalytic activity

Nayeli Fabiola Ibarra-Cervantes<sup>1</sup> · Edgar Vázquez-Núñez<sup>1</sup> · Christian Gómez-Solis<sup>2</sup> · Fabian Fernández-Luqueño<sup>3</sup> · Gustavo Basurto-Islas<sup>2</sup> · Jonathan Álvarez-Martínez<sup>2</sup> · Rigoberto Castro-Beltrán<sup>2</sup>

Received: 14 September 2023 / Accepted: 4 January 2024 / Published online: 19 January 2024  
© The Author(s), under exclusive licence to Springer-Verlag GmbH Germany, part of Springer Nature 2024

## Abstract

Green synthesis (GS), referred to the synthesis using bioactive agents such as plant materials, microorganisms, and various biowastes, prioritizing environmental sustainability, has become increasingly relevant in international scientific practice. The availability of plant resources expands the scope of new exploration opportunities, including the evaluation of new sources of organic extracts, for instance, to the best of our knowledge, no scientific articles have reported the synthesis of zinc oxide nanoparticles (ZnO NPs) from organic extracts of *T. recurvata*, a parasitic plant very common in semiarid regions of Mexico. This paper presents a greener and more efficient method for synthesizing ZnO NPs using *T. recurvata* extract as a reducing agent. The nanoparticles were examined by different techniques such as UV–vis spectroscopy, X-ray diffraction, scanning electron microscopy (SEM), Fourier transform infrared spectroscopy (FTIR), X-ray photoelectron spectroscopy (XPS), and BET surface analysis. The photocatalytic and adsorptive effect of ZnO NPs was investigated against methylene blue (MB) dye in aqueous media under sunlight irradiation considering an equilibrium time under dark conditions. ZnO nanoparticles were highly effective in removing MB under sunlight irradiation conditions, showing low toxicity towards human epithelial cells, making them promising candidates for a variety of applications. This attribute fosters the use of green synthesis techniques for addressing environmental issues.

This study also includes the estimation of the supported electric field distributions of ZnO NPs in their individual spherical or rounded shapes and their randomly oriented organization, considering different diameters, by simulating their behavior in the visible wavelength range, observing resonant enhancements due to the strong light-matter interaction around the ZnO NPs boundaries.

**Keywords** Green synthesis · Non-conventional biomass · Water pollution, Metallic nanoparticles · Photocatalysis

## Introduction

Plants belonging to the genus *Tillandsia* are found in various ecosystems, including equatorial tropical forests, high-elevation mountains, and rock-dwelling swamps. These plants typically grow in cold and humid climates under shade and at lower forest levels (Luna-Cozar et al. 2020). This plant grows prominently on two *Fabaceae* family members, hui-zache (*Acacia* spp.), and mesquite (*Prosopis* spp.), which are ecologically significant due to their ability to fix nitrogen, conserve soils, and restore degraded soils (Zapata-Campos et al. 2020).

Moreover, owing to their unique ecological niche, plants belonging to the genus *Tillandsia* have been found to contain a diverse array of molecules biologically active found

Responsible Editor: George Z. Kyzas

✉ Edgar Vázquez-Núñez  
edgar.vazquez@ugto.mx; ed.vazquezn@gmail.com

<sup>1</sup> Departamento de Ingenierías Química, Electrónica y Biomédica, División de Ciencias E Ingenierías, Grupo de Investigación Sobre Aplicaciones Nano y Bio Tecnológicas Para La Sostenibilidad (NanoBioTS), Universidad de Guanajuato, Lomas del Bosque 103, Lomas del Campestre, C.P. 37150 León, Guanajuato, Mexico

<sup>2</sup> Division of Sciences and Engineering, University of Guanajuato, León, México

<sup>3</sup> Sustainability of Natural Resources and Energy Program, C.P. 25900 Cinvestav-Salttillo, Coahuila, Mexico

in plants, also called phytochemical (Bitwell et al. 2023) that exhibit antiviral, antitumor, and antibacterial activities (Pérez-López et al. 2020; Lasso et al. 2022; Lo et al. 2022).

Nanoparticles (NPs) are defined as a group of particles having sizes between 1 and 100 nm and characterized by some specific physicochemical properties such as surface area, surface charge, degree of agglomeration, particle morphology, and surface coating (Turan et al. 2019; Cai et al. 2020).

As a result, these properties have enabled their application in various fields, including but not limited to, environmental remediation processes, drug delivery systems, and pharmacology as carriers of chemical compounds (Tosi et al. 2020). Intending to minimize the environmental impact, GS has emerged as a promising alternative to conventional methods of synthesizing NPs that are known to be highly polluting and generate numerous chemical residues, while also being associated with decreased biocompatibility due to their toxicity (Salem and Fouda 2021).

Metallic nanoparticles or metal nanoparticles is a term that refers to nanoparticles synthesized using metals such as gold, silver, platinum, or zinc (Jamkhande et al. 2019; Gudkov et al. 2021). The synthesis methods of metal nanoparticles include physicochemical sol–gel method (Parashar et al. 2020), sol–gel combustion method (Tolossa and Shibeshi 2022), chemical synthesis (Muthuvel et al. 2020), mechanical method (Yusof et al. 2019), and green synthesis methods where are mainly used organic extracts from plants as reducing agents (Verma et al. 2021).

Among metal nanoparticles, Zn NPs are interesting because of their impressive properties, including a wide band gap, large binding energy, and high piezoelectric properties (Uribe-López et al. 2021). Zinc oxide (ZnO) NPs synthesized using green methods can exhibit a wide variety of nanostructures and have been demonstrated to be safe, non-toxic, and biocompatible (Mirzaei and Darroudi 2017; Faisal et al. 2021). They have been used in various technologies and industries such as optoelectronics, sensors, biology, medicine, and environmental restoration (Sadiq et al. 2021; Islam et al. 2022). ZnO NPs are widely used as semiconductors with a band gap of 3.37 eV and an exciton binding energy of 60 meV (Kumbhar et al. 2019), making them one of the best photocatalysts to degrade contaminants in water due to their capacity for photooxidizing chemical and biological species (Deak et al. 2019). Besides their photocatalytic activity, ZnO nanoparticles also can adsorb chemical compounds in water, for instance, Omar et al. (2014) reported the use of ZnO nanoparticles as both adsorbent and photocatalyst to remove MB from an aqueous solution. Several studies have reported this effect, i.e., adsorptive and photocatalytic of ZnO NPs for removing different contaminants present in water, e.g., 4-nitrophenol (Bhatia and Nath 2020), methylene blue (Sadiq et al. 2021), anthracene

(Hassan et al. 2015), methyl orange (Gherbi et al. 2022), 2,4-dinitrophenol (Nouri-Mashiran et al. 2022), and cationic and anionic dyes (Sasi et al. 2022).

Recently, *T. recurvata* has overpopulated and infested endemic species of huizache and mesquite trees, leading to a significant reduction in their population in the Mexican plateau states, significantly altering their ecosystems and ecological functions. Some local Mexican governments have implemented tree-pruning campaigns to physically eliminate *T. recurvata*, generating a significant amount of biomass without any potential benefits and representing costs for its management and final disposal. Therefore, this residual biomass has been evaluated as a raw material for introduction into diverse processes.

Various techniques are currently being investigated to produce nanoparticles while minimizing the production of chemical waste. GS has been identified as an environmentally responsible option. In this study, ZnO NPs were produced using organic extracts of *T. recurvata* in a simple and environmentally friendly manner. To evaluate the photocatalytic properties of the synthesized nanoparticles, MB solutions containing ZnO NPs were first equilibrated at dark conditions and then exposed to sunlight. In addition to the physicochemical characterization of the NPs, a computational simulation was used to estimate the plasmonic response at the range of wavelength values, and finally, the WST-1 assay was used to assess the viability of HCT-15 cells.

## Materials and methods

Analytical-grade materials were used without further purification. All solutions were prepared using double-distilled water. The analysis and measurements were performed using various advanced systems and tools, including a UV–visible spectrophotometer (UV–vis DRS), FTIR Spectrometer (Nicolet 6700), X-ray diffraction system (XDR, Smart Lab Rigaku), field emission scanning electron microscope (FE-SEM, model JSM-7800F PRIME). Brunauer-Emmet-Teller (BET, Quantachrome NOVA 2000e). The photodegradation process was monitored by the photoluminescence method using a spectrofluorometer FLUOROLOG-FL3-111 (Horiba). Cell viability was determined by employing a plate reader (Thermo Scientific, Waltham, MA, USA).

## Plant collection

*T. recurvata* specimens were collected manually from a natural ecosystem in the municipality of Tula de Allende, Hidalgo, Mexico (20°0'36.995"N 99°21'19.325"O) between February and June. The average temperature at the site was

recorded as 16.2 °C, with an annual precipitation value of 674 mm (INEGI, 2023).

### Extraction of *T. recurvata* phytochemicals

The *T. recurvata* plants were washed and disinfected to eliminate residual soil and other particles. Subsequently, the plant material was oven-dried for 24 h at 40 °C. The dried plant material was ground into a fine powder and stored at room temperature. In a beaker, a dissolution consisting of 3 g of *T. recurvata* powder and 200 ml of distilled water was prepared. After 30 min of heating at 60°C, the mixture was filtered by gravity. For future use, the extracts were stored at a temperature of –4 °C.

### Qualitative phytochemical screening

Qualitative analysis was done using a fresh organic fraction of *T. recurvata* and using standard methods. The tests were considered as positive when was observed the presence of precipitates or change of color. A general description of the tests is shown as follows:

#### Test for carbohydrates

**Molisch test** The crude extract was mixed with 2 ml of Molisch's reagent, and the mixture was shaken properly. After that, 2 ml of concentrated H<sub>2</sub>SO<sub>4</sub> was poured carefully along the side of the test tube. The appearance of a violet ring at the interphase indicated the presence of carbohydrates (Purewal et al. 2023).

#### Test for flavonoids

**Flavonoid test** The crude extract was mixed with a few fragments of magnesium ribbon and concentrated HCl was added dropwise. The pink scarlet color appeared after a few minutes which indicated the presence of flavonoids (Kirana et al. 2023).

#### Test for tannins

Crude extract was mixed with 2 ml of 2% solution of FeCl<sub>3</sub>. A blue-green or black coloration indicated the presence of tannins (Jigna and Sumitra 2008).

#### Test for saponins

**Foam test** The crude extract was mixed with 5 ml of distilled water in a test tube and it was shaken vigorously. The formation of stable foam was taken as an indication of the presence of saponins (Tan et al. 2023).

### Test for anthraquinone

**Borntrager test** Extraction of *T. recurvata* with KOH at 5% was filtered and acidified. The extract was mixed with benzene and several drops of NH<sub>4</sub>OH were added and stirred. The presence of a pink to red coloration represents the presence of anthraquinone (Dhiman et al. 2023).

### Test for alkaloids

**Dragendorff test** The crude extract of *T. recurvata* was mixed with several drops of Dragendorff reagent and stirred. A shift in extracts' color from pale to brown indicates that there is an alkaloid (Merakeb et al. 2023).

### Test for terpenoids

**Salkowski test** The crude extract was mixed with 2 ml of chloroform. Then, 2 ml of concentrated H<sub>2</sub>SO<sub>4</sub> was added carefully and shaken gently. A reddish brown color indicated the presence of a steroidal ring, i.e., the glycone portion of the glycoside (Khan et al. 2023).

### Test for reducing sugars

**Fehling test** An equal volume of Fehling A and Fehling B reagents were mixed and 2 ml of it was added to crude extract and gently boiled. A brick-red precipitate appeared at the bottom of the test tube indicating the presence of reducing sugars (Thamer et al. 2023).

### Green synthesis of ZnO NPs

Zinc chloride (ZnCl<sub>2</sub>) weighing 3.4 g and 50 ml of the aqueous extract of *T. recurvata* were combined in a beaker and heated to 80 °C for 1 h leading to the formation of a dark brown precipitate. This precipitate was separated from the reaction mixture by vacuum filtration using Whatman® No. 1 filter paper (particle retention of 11 µm). The collected solids were dried at 70 °C for 12 h. To investigate the impact of the synthesis conditions on the nanoparticle structure, the dried solids were calcined at 300 °C, 500 °C, and 700 °C in a muffle furnace for 1 h. The final product was stored at room temperature, while the generated residues were collected and properly disposed of.

### Characterization of ZnO NPs

The ZnO NPs were characterized using several analytical techniques including X-ray diffraction (XRD), Fourier-transform infrared spectroscopy (FTIR), field-emission scanning electron microscopy (FESEM), energy-dispersive X-ray spectroscopy (EDS), and UV–vis spectroscopy. The

surface area of ZnO NPs was determined by the Brunauer-Emmet-Teller (BET) and pore size and pore volume analysis was done by the Barret-Joyner-Halenda (BJH) method (Modi and Fulekar 2020).

### Photocatalytic activity

The synthesized ZnO NPs were evaluated for their ability to photodegrade MB under sunlight irradiation. For the photodegradation analysis, solutions containing known concentrations of MB and the photocatalyst were prepared and allowed to equilibrate for 60 min in darkness. The photodegradation process was carried out in 100 mL glass Erlenmeyer flasks, the units were set up in triplicate, resulting in a total of 9 units per treatment. The control treatment consisted of the same MB concentration but without the addition of ZnO NPs.

After equilibration time, the flasks were exposed to sunlight for 180 min to promote photodegradation, and aliquots were collected for analysis at time points of 0, 10, 30, 60, 120, 150, and 180 min. The samples were centrifuged at 4000 rpm for 10 min, and the MB concentration was measured using UV spectrophotometry.

The MB degradation was measured using the following equation:

$$\text{Percentage of degradation} = \frac{C_0 - C_t}{C_0} \times 100$$

where  $C_0$  is the initial absorbance of the dye solution and  $C_t$  is the absorbance of MB after time  $t$  in min.

### Evaluation of supported electric field distributions by COMSOL modeling

The effect of the electric field distributions created by light-matter interactions of the incident light, ZnO-NPs, and the surrounding medium (distilled water) is studied at different wavelengths, different Zn-NPs diameters, and different Zn-NPs presentations in silico experiments through COMSOL-Multiphysics software. 2D Simulations were performed via the physics module, while the localized surface plasmon resonances (LSPR) were solved via the electromagnetic waves and the frequency domain modules; resulting in the observable maximum supported  $|E|^2$  surrounding the

ZnO NPs. All simulations were performed on the nanometer scale.

To emulate the experiments (visible region of the solar spectral irradiance), 2D simulations were performed by establishing two main working wavelengths (360 nm and 750 nm). A free triangular mesh size of 1.2 nm was employed for all the simulations. In addition, several animations are presented in Supplementary information 1, where the study considered a broader spectral region from 300 to 1000 nm. Table 1 summarizes the parameters used to perform these simulations.

### Determination of the degradation mechanism mediated by ZnO NPs

To understand the role of ZnO NPs in photodegradation, the following experiment was carried out. The experiment consisted of a 0.4-mM terephthalic acid (TA) dissolved in distilled water with 2 mM NaOH along with 20 mg of ZnO NPs; TA reacts in the presence of the nanoparticles in the aqueous dissolution generating  $\bullet\text{OH}$  radicals to produce 2-hydroxyterephthalic acid. This process was followed by the photoluminescence method using TA as a marker (Jayaraj et al. 2018).

### Cell culture and cell viability assay

HCT 15 cells, which are isolated from the large intestine (American Type Culture Collection, ATCC) were grown in a 100-mm cell culture Petri dish at 37 °C with 5%  $\text{CO}_2$  in RPMI cell culture medium containing amino acids, vitamins, phosphate, sodium bicarbonate, and supplemented with 10% fetal bovine serum. The effect of nanoparticles on cell viability was analyzed using a water-soluble tetrazolium salt (WST-1) assay, following the manufacturer's instructions (Abcam, Cambridge, UK). Briefly,  $5 \times 10^4$ /well cells were cultured in a 96-well microtiter plate at a final volume of 100  $\mu\text{L}$  per well for 24 h prior to the experiment. The cells were incubated for 24 h with ZnO NPs at concentrations of 50  $\mu\text{g}/\text{mL}$ , 70  $\mu\text{g}/\text{mL}$ , and 100  $\mu\text{g}/\text{mL}$ . Afterward, WST-1 reagent was added to each well and incubated under standard culture conditions for 1 h. The

**Table 1** Material parameters considered for simulations

Materials properties	Distilled water	ZnO-NPs	References
$\epsilon_r$	1.77	3.50	(Archer and Wang 1990)
$\mu_r$	1.00	1.00	(Goda and Behrenbruch 2004)
$\sigma$	$5 \times 10^{-6}$	$1 \times 10^2$	(Hermans et al. 2014; Baxter and Schmuttenmaer 2006)

$\epsilon_r$  relative permittivity,  $\mu_r$  relative permeability,  $\sigma$  conductivity [S/cm]

absorbance of the samples was measured using a microtiter plate reader (Thermo Scientific, Waltham, MA, USA) at 440 nm. Non-treated cells were used to control cell viability.

## Statistical analysis

The tests for MB removal, cell viability, and phytochemistry were conducted in triplicate. To determine the efficacy of ZnO NPs, an analysis of variance (ANOVA) was conducted on MB removal and cell viability. The statistical significance of the observed probability values ( $p < 0.05$ )

**Table 2** Phytochemical screening of *T. recurvata* extract

Metabolite	Test	Result	Reference
Carbohydrates	Molisch test	(+++)	(Purewal et al. 2023)
Flavonoids	Shinoda test	(++)	(Kirana et al. 2023)
Tannins	Stiasny test	(+++)	(Kilpeläinen et al. 2023)
Saponins	Foam test	(++)	(Tan et al. 2023)
Anthraquinone	Borntrager test	(—)	(Dhiman et al. 2023)
Alkaloids	Dragendorff test	(++)	(Merakeb et al. 2023)
Terpenoids	Salkowski test	(++)	(Khan et al. 2023)
Reducing sugars	Fehling test	(+++)	(Thamer et al. 2023)

—=No detected; + = low; ++ = moderate; +++ = strong

was considered significant and estimated using the General Linear Model procedure (PROC GLM; SAS 1989).

## Results and discussion

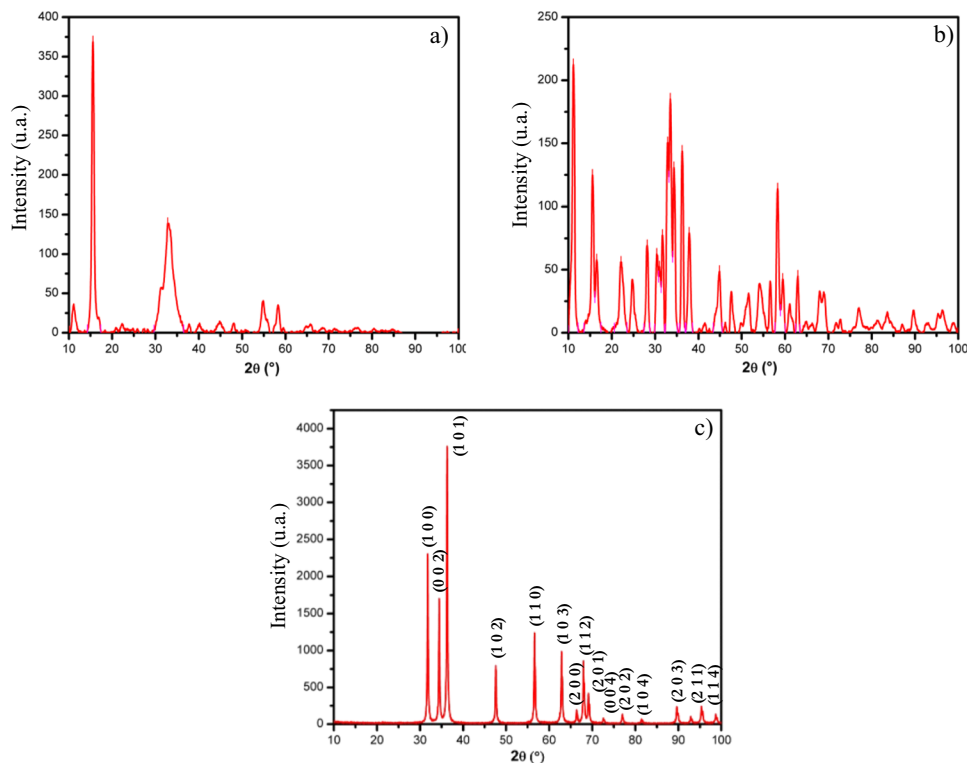
### Phytochemical screening of *T. recurvata* extracts

The results of the phytochemical analyses are presented in Table 2. The organic fraction exhibited positive results for tannins, reducing sugars, and carbohydrates, which are essential reducing compounds that act as reducing agents to promote the formation of oxide metallic NPs. The phytochemicals also play a critical role in the metabolic processes of plants, for instance, Bellotti and Deyá (2019), reported that tannins can reduce zinc (Zn) ions to their lower oxidation states, and Hamidian et al. (2022) confirmed that alkaloids extracted from *Salvatore persica* efficiently promoted the synthesis of ZnO NPs which showed excellent physical properties and minimum toxicity effect to MCF-10A cell line.

### Diffraction of X-ray (XDR)

The XDR patterns of the green-synthesized ZnO NPs annealed at 300, 500, and 700 °C are presented in Fig. 1a–c, respectively. The diffraction peaks ( $2\theta$ ) for the material annealed at 700 °C, i.e., 31.8°, 34.4°, 36.2°, 47.6°, 56.6°,

**Fig. 1** Diffraction patterns of materials synthesized and annealed for 1 h at different temperatures: **a** 300 °C, **b** 500 °C, and **c** 700 °C





62.9°, 67.9°, 68.5°, 69.2°, 72.5°, 76.4°, 81.5°, 89.5°, 93.1°, 96.01, and 97.6°, corresponding to the planes (1 0 0), (0 0 2), (1 0 1), (1 0 2), (1 1 0), (1 0 3), (2 0 0), (1 1 2), (2 0 1), (1 0 4), (2 0 2), (1 0 5), (2 1 1), (2 1 2), (2 1 3), and (3 0 0), confirmed the formation of wurtzite (hexagonal close-packed structure) which is a type of close packing of a sphere in three dimensions. The average crystallite size of the ZnO NPs was determined by the Debye–Scherrer formula and was found to be 26.77 nm. In various experiments using green synthesis methods, ZnO nanoparticles of comparable size demonstrated photocatalytic activity with high removal efficiency of chemical compounds in aqueous media (Anbuvaran et al. 2015; Shah et al. 2019; Fouda et al. 2022). The crystallite size was determined as follows:

$$D = \frac{0.9\lambda}{\beta \cos\theta}$$

where  $\lambda$  is the X-ray wavelength of Cu–K $_{\alpha}$  radiation (1.5406 Å),  $\beta$  is the full width at half maximum (in radians), and  $\theta$  is the Bragg angle.

### Morphology studies by field emission scanning electron microscopy (FE-SEM)

Previous studies have evaluated the influence of diverse factors on the morphology and properties of ZnO nanoparticles synthesized via green synthesis, obtaining spherical crystallite sizes ranging from 11.35 to 65 nm, using various plant extracts, including *Brassica oleracea*, *Syzygium cumini*, and *Moringa oleifera*, among others (Matinise et al. 2017; Osuntokun et al. 2019; Sadiq et al. 2021). Among the investigated parameters, annealing temperature emerged as one of the most crucial for obtaining defined morphologies. FE-SEM was used to examine the morphologies of the synthesized products. Figure 2 depicts the results of annealing temperatures of (a) 300 °C, (b) 500 °C, and (c) 700 °C. The images reveal various degrees of agglomeration of the amorphous material (Fig. 2a), a more defined morphology with a flake-like structure (Fig. 2b), and well-defined nanoparticles ranging

in diameter from 12 to 61 nm (Fig. 2c). At 700 °C, spherical nanoparticles were observed, which is a common shape for ZnO NPs synthesized applying GS. For example, Thi et al. (2020) demonstrated that a better morphology and photocatalytic activity of green synthesized ZnO NPs were improved when the annealing process was performed at a higher temperature i.e., 600 °C, similar studies confirmed that the morphology crystallinity, and size of the ZnO NPs were temperature-dependent (Kabir et al. 2019). Later results of FTIR and EDS analysis supported that high annealing temperature, i.e., 700 °C is crucial for obtaining the desired shape and morphology of ZnO NPs with high photocatalytic efficiency.

### Energy dispersive spectroscopy (EDS)

The chemical composition (Zn, O, and other trace elements) of the prepared ZnO NPs was observed by energy dispersive spectroscopy (EDS) analysis, and the results are presented in Table 3. Unlike at lower temperatures, the percentage of impurities such as chlorine and other elements (Al, Si, phosphorus, sulfur, and Ca) decreases at 700 °C. This confirms that the annealing temperature is crucial for obtaining high-purity nanoparticles contributing to better properties and performance.

Based on these results, it can be inferred that over a certain time and as the annealing temperature increases, structural defects (likely caused by the presence of residual compounds from the reaction process) are reduced, and therefore, the morphology of the particles that make up the material becomes more defined. It has been proved that higher annealing temperature produces a higher compressive

**Table 3** Elemental composition of samples annealed at different temperatures

Temperature (°C)	Elemental composition (%)			
	Zn	O	Cl	Other
300	35.964	51.507	11.549	0.98
500	35.553	48.198	15.908	0.341
700	47.826	50.995	0.861	0.318

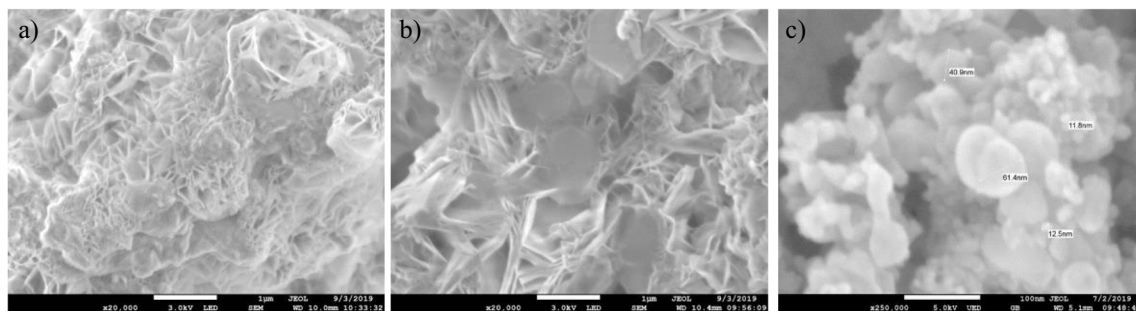


**Fig. 2** Morphology of the material annealed at different temperatures **a** 300 °C, **b** 500 °C, and **c** 700 °C

stress on the NPs affecting not only the morphology but their chemical composition (Nagamalleswari and Modem 2023).

### Fourier Transform Infrared Spectroscopy (FTIR)

Figure 3 shows the FTIR spectra of the ZnO NPs annealed at three different temperatures. The vibration of the O–H bond of water absorbed on the surface was linked to the large band at  $3466\text{ cm}^{-1}$  and a smaller band at  $1603\text{ cm}^{-1}$  (Thamer et al. 2023). According to Kumar et al. (2019), the band at  $2091\text{ cm}^{-1}$  showed double carbon bonds with other elements (such as nitrogen or sulfur), while the peak at  $1414\text{ cm}^{-1}$  was attributed to the C=O bond. In addition, the band at  $2342\text{ cm}^{-1}$  was assigned to atmospheric  $\text{CO}_2$  absorption by  $\text{Zn}^{2+}$  metal cations. These peaks may have been caused by the organic components of the *T. recurvata* extract (Khan et al. 2018).

In the sample calcined at  $700\text{ }^\circ\text{C}$ , a band corresponding to the link between zinc and oxygen was observed at  $918\text{ cm}^{-1}$ . According to Chaudhari and Kale (2017), metal oxides typically exhibit absorption bands in the fingerprint

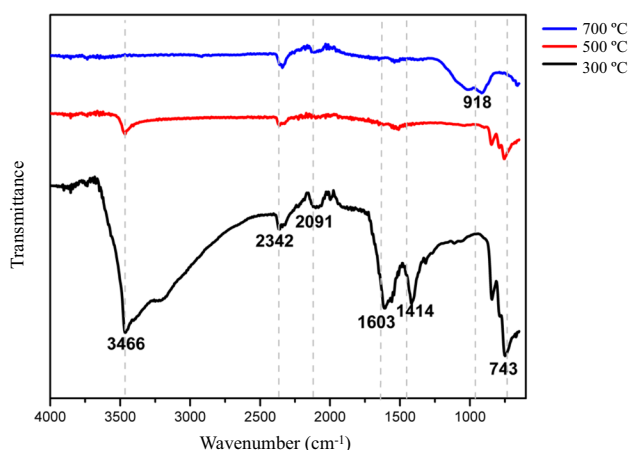
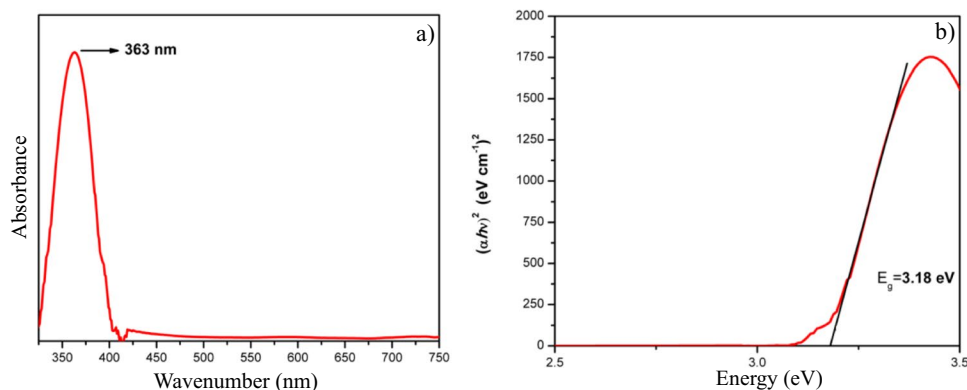


**Fig. 3** FTIR spectra of the products calcined at three different temperatures

**Fig. 4** Band gap determination of synthesized ZnO NPs through UV–vis absorption spectrum



region (i.e., below  $1000\text{ cm}^{-1}$ ) owing to vibrations between the atoms involved, proving that the annealing temperature is crucial for producing defined nanoparticles with a high degree of purity.

The findings demonstrated that some of the peaks detected at  $300\text{ }^\circ\text{C}$  dramatically decreased at  $500\text{ }^\circ\text{C}$  and  $700\text{ }^\circ\text{C}$ .

This shows that the removal of contaminants from the nanoparticles, which may impair their photocatalytic efficacy and potentially harm living organisms and the environment, depends critically on the annealing temperature.

### UV–vis absorbance

The UV–vis absorption spectrum of the ZnO NPs annealed at  $700\text{ }^\circ\text{C}$  (used for the photocatalytic process) is shown in Fig. 4, where a peak of maximum absorbance at  $363\text{ nm}$  was observed. The method proposed by Tauc and Menth (1972) was used to determine the width of the optical bandgap.

$$(\alpha h\nu)^{1/n} = k(h\nu - E_g)$$

where  $\alpha$  is the absorption coefficient,  $h\nu$  is the energy of the incident photon,  $k$  is a constant independent of energy,  $E_g$  is the energy of the optical band gap, and  $n$ , known as the transition mode power factor, depends on the nature of the material (i.e., whether it is crystalline or amorphous) and can take values of  $1/2$ ,  $2$ ,  $3/2$ , or  $3$ , depending on whether it is a direct allowed, indirect allowed, direct forbidden, or indirect forbidden transition, respectively (Sharma et al. 2022).

An energy equation was used to calculate photon energy. In this case, the frequency of the incident photon ( $\nu$ ) can be replaced with the value of the speed of light ( $c$ ) divided by the wavelength of the photon ( $\lambda$ ), and as a result, it is possible to calculate the optical band gap ( $E_g$ ) (Ibañez et al. 1991).

The photon energy ( $h\nu$ ) is plotted on the  $x$ -axis, and the parameter  $(\alpha h\nu)$  is plotted on the  $y$ -axis, according to the Tauc method. It is worth noting that for ZnO, the transition

is a direct allowed transition; therefore, the value of  $n$  is  $\frac{1}{2}$  (Kamarulzaman et al. 2015). The linear portion of the resulting curve was extrapolated to the  $x$ -axis (where  $\alpha=0$ ), and the value of the optical band gap was obtained as 3.18 eV, which is slightly lower than the reported literature value. of 3.20–3.37 eV (Limpachanangkul et al. 2019).

The graphs in Fig. 4 show (a) the UV–vis absorption spectrum for the annealed nanoparticles and (b) the energy of the photon ( $h\nu$ ) on the  $x$ -axis and the parameter ( $\alpha h\nu$ ) on the  $y$ -axis according to the previously mentioned method.

**BET analysis**

The BET surface area of samples was measured by  $N_2$  adsorption isotherms. The specific surface area of ZnO NPs was determined by the BET method. This method involved the physical adsorption of  $N_2$  at its boiling temperature. The following equation is used to find out surface area by BET method (Gatou et al. 2022)

$$\frac{P}{Va(Po - P)} = \frac{1}{VmC} + C - \frac{1}{VmC} \times \frac{P}{Po}$$

where,  $P$  = adsorption equilibrium pressure,  $Po$  = Saturated vapor pressure of adsorbate,  $Va$  = volume of adsorbate required for a monolayer coverage, and  $C$  = A constant relating to the head of adsorption.

As per the BET method, a plot  $P/Va(Po-P)$  against  $P/Po$  yields a straight line when  $\frac{P}{Po} < 0.3$ . The  $Vm$  value is obtained from the slope and intercept of the straight line by following the equation.

$$SurfaceArea \frac{m^2}{g} = Vm \times \frac{N}{22414 \times W} \times Am$$

where,  $Vm$  = monolayer volume in ml at standard pressure and temperature (STP);  $N$  = Avogadro number;  $W$  = weight of the powered sample (g);  $Am$  = cross-sectional area of adsorbate molecule ( $0.162 \text{ nm}^2$  for  $N_2$ ).

According to the data, the surface area for the ZnO NPs is  $13.01 \text{ m}^2\text{g}^{-1}$ , the pore radius is  $1.52 \text{ \AA}$ , and  $0.023$  for the pore volume ( $\text{cc/g}$ ).

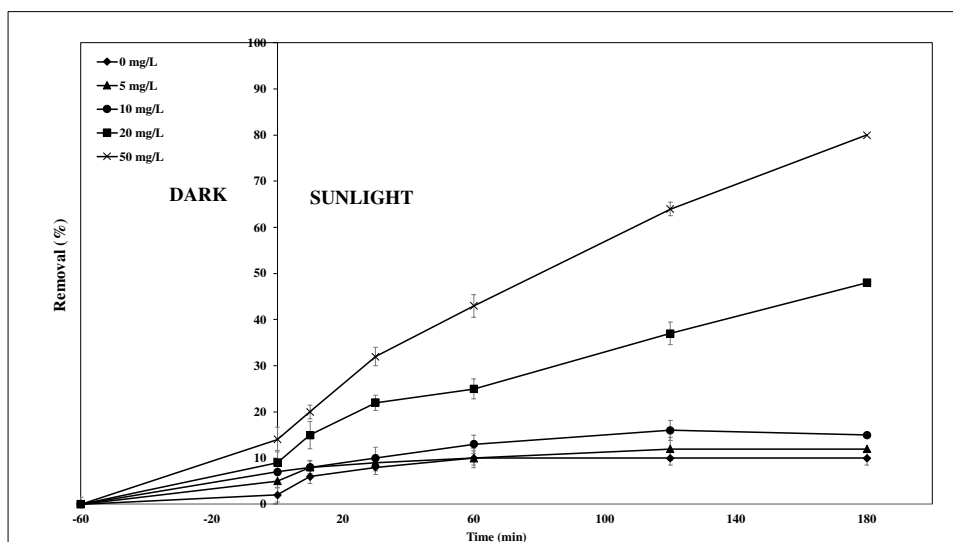
**Photocatalytic degradation of methylene blue: Influence of amount of ZnO NPs and MB**

The optimal photocatalyst dosage for the removal percentage of MB was assessed by altering the quantity of ZnO NPs from 5.0 to 50 mg/L, while the 20 mg/L dye concentration and pH 7 remained unaltered. The results revealed that the removal efficacy of MB was considerably influenced by the amount of photocatalyst, as shown in Fig. 5.

The results demonstrate that a higher initial concentration of ZnO NPs was observed in a higher MB removal percentage. After equilibrium time, it was reduced the initial concentration of MB; this result can be explained by the adsorptive capacity of the ZnO nanoparticles.

As part of this work, it was necessary to eliminate the interference due to the adsorption effect since it is known that the adsorptive capacity of dye molecules on the surface of the photocatalyst is a crucial factor that influences the photocatalytic performance of the catalyst. For instance, Lal et al. (2022) evaluated the combined photocatalytic and adsorptive effect of green synthesized ZnO NP to remove MB from aqueous media, observing that the NPs exhibited better photocatalytic activity due to their better adsorption capacity reaching 91% of MB degradation after 180 min of sunlight exposure. In a similar experiment, Nguyen et al. (2021) evaluated the adsorption and photocatalytic performance of ZnO NPs fabricated from *Canna indica* L. flowers

**Fig. 5** Removal of MB during photocatalysis with ZnO nanoparticles at different concentrations under dark (60 min) and sunlight conditions (3 h in a day)





extract for removing organic dyes, observing that the dye molecules behaved monolayer adsorption on ZnO surface layers and that this process it was controlled by chemisorption. The study reported that sunlight was effective for photocatalytic degradation of MB using green synthesized ZnO NPs (94.23% removal and 31.09 mg/g of uptake capacity). Our results showed a reduction of the initial concentration of MB during the dark equilibrium stage, proving that ZnO NPs can present adsorptive behavior which is positively correlated to the amount of the photocatalyst, i.e., at 50 mg/L of ZnO NPs it was observed a 20% removal of MB, 15% removal for 20 mg/L of ZnO NPs, 7% removal for 10 g/L, and 5% for 5 mg/L, observing statistical difference only between the higher ZnO NPs concentration (50 mg/L) with lower concentrations (0 mg/L to 20 mg/L). It has been reported that ZnO NPs show a low capacity to adsorb compared to their composites or other metallic nanomaterials (Nang An et al. 2020; Obayomi et al. 2021).

After the equilibrium time, the removal efficiency was significantly higher for samples with ZnO concentrations of 20 and 50 mg/L, with removal values of 30% and 80%, respectively, after 3 h of sunlight exposure. The removal obtained for experiments with ZnO concentrations of 0, 5, and 10 g/L did not show significant statistical differences. A gradual decrease in the absorption band was observed in the experiments with 20 g/L and 50 g/L ZnO nanoparticles, indicating the breaking of the conjugated system by hydroxyl radicals generated through photocatalysis, causing the formation of smaller organic compounds (Krishnan et al. 2023). Figure 6 shows the results obtained.

The influence of the initial MB concentration was analyzed by preparing solutions of this dye at concentrations of 0, 5, 10, 20, and 50 mg/L of the ZnO catalyst and an initial MB concentration of 50 mg/L. The MB dye exhibited an absorption band with two peaks at 612 and 664 nm,

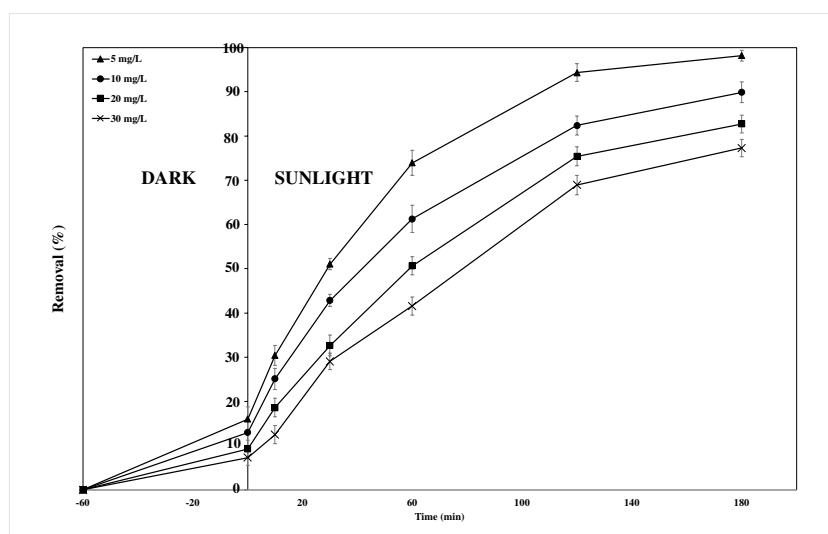
corresponding to the conjugated system formed between sulfur and nitrogen, which acted as a chromophore in the molecule (Renda et al. 2021). In the absence of ZnO nanoparticles, MB is generally stable, and the rate of its degradation under sunlight is 8%; similar results were observed by (Vasiljevic et al. 2020). Results are shown in Fig. 5.

The impact of dye concentrations on the removal performance of the MB was also assessed by changing the dye concentration from 5.0 to 30.0 mg/L using sunlight irradiation while maintaining the photocatalyst amount at 20 mg/L and pH 7 as shown in Fig. 6. It was observed that the adsorptive performance of ZnO nanoparticles during the dark conditions experiment was greater at lower concentrations of MB ranging from 16% of removal for 5 mg/L MB to 7% of removal for 30 mg/L); this can be explained by the saturation of the photocatalyst surface, being this the predominant process during the dark exposure (Elmorsi et al. 2017; Nang An et al. 2020).

The results showed that the photocatalytic performance of the ZnO NPs was inversely proportional to the MB concentration, that is, the maximum removal of MB was obtained at a minimum concentration of MB (5 and 10 mg/L). It was also noticed that when MB increased from 10 to 30 mg/L, MB-removal gradually decreased from 100 to ~80%. This abatement is due to the decreased light absorption on the photocatalyst surface with increasing dye concentration, which in turn reduces the production of OH<sub>2</sub> radical ions that have been reported to play a crucial role in the photodegradation process (Nguyen et al. 2018).

In general, similar removal results were obtained for green-synthesized ZnO nanoparticles using several plant extracts, such as *S. cumini*, *Myristica fragans* (Faisal), and *Scutellaria baicalensis* (Chen et al. 2019).

**Fig. 6** Removal of MB at different initial concentrations during photocatalysis with ZnO nanoparticles under dark conditions (60 min) and sunlight irradiation (3 h in a day)



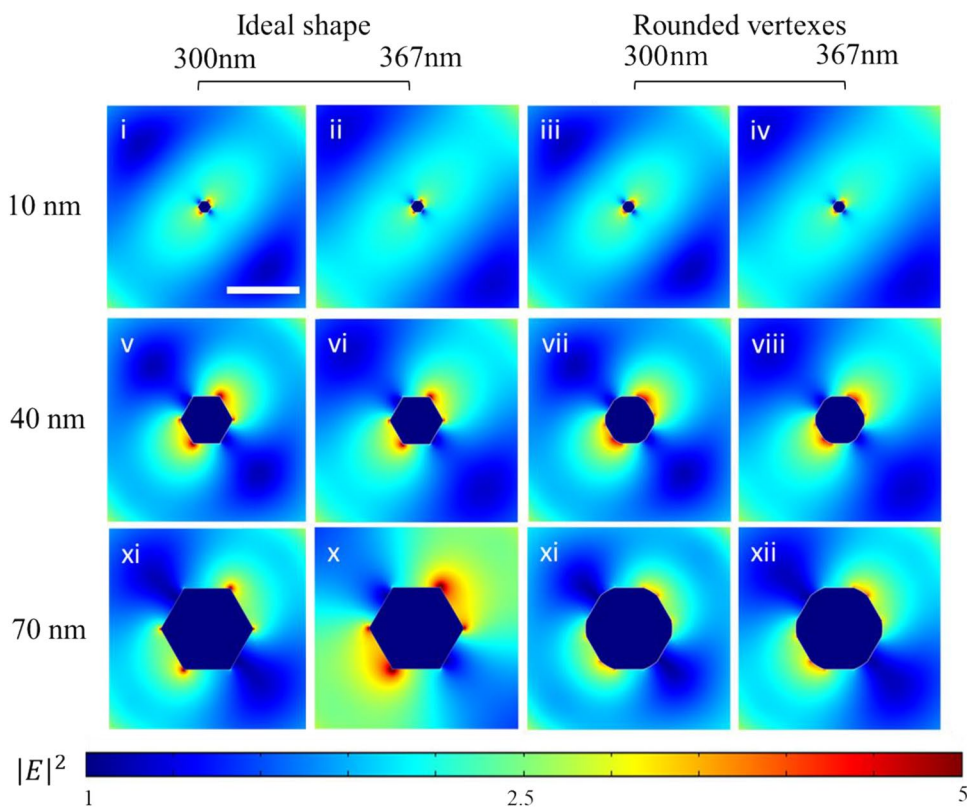
## ZnO–NPs simulations

In Fig. 7,  $|E|^2$  simulations are shown for ideal geometrical wurtzite hexagonal single ZnO NPs at different diameters and for those with rounded vertexes emulating the observable SEM images presented above. Simulations in Fig. 7 (from i to xii) show that at different wavelengths and diameters, the  $|E|^2$  profiles vary along the immediate surrounding medium. For example, under 360 nm wavelength excitation, the observable hot spots are more confined to smaller surface regions for all cases, while at 365 nm, longer LSPR is distributed around ideal and rounded vertexes and edges. In addition, for both wavelengths, the rounded configurations slightly reduced the LSPR amplitudes. Regardless of the shape configuration (ideal and/or rounded), the electric field enhancements are located at the vertexes and edges of the ZnO–NPs. Previously, metallic oxide semiconductor nanostructures (ZnO–NPs) have been used as potential systems for SERS applications (Marica et al. 2022; Li et al. 2023) demonstrating their versatility in terms of promising materials for electron mobility under longer excitation wavelength range. For example, optical excitation ranging along the near-IR results in electronic excitation in the conduction band, while those regions centered along the UV, result in electronic excitation in the valence band (Li et al. 2023). This electronic mobility is finally understood such as the collective resonance of surface plasmons generated

and oscillating under the influence of incident EM fields in a broader wavelength range.

Because the physical properties of nanomaterials strongly depend on their morphology and their topology presentations, an example of the resonant plasmonic enhancement distributions for different ZnO–NPs ensembles distributed in a surface area of 400 nm × 400 nm with different diameters, is presented in Fig. 8.  $|E|^2$  simulations are done at four different wavelengths revealing that whatever the working wavelengths, the maximum  $|E|^2$  values are supported along the ZnO–NPs surroundings; demonstrating the plasmonic resonant enhancements due to the strong light-matter interaction around the ZnO–NPs boundaries. These  $|E|^2$  simulations show, in addition, that under these randomly oriented ZnO–NPs, the maxima plasmonic enhancements are observed along all working wavelengths; showing, in addition, that at shorter wavelengths the LSPRs are supported more on that region for small ZnO–NPs, while at 750 nm, the LSPRs are located where ZnO–NPs with greater diameters are. It is well known that the optical properties of NPs are strongly influenced by their sizes. This dependence is not exclusive to those NPs based on metallic and organic; semiconductor-based NPs also present modifications in their optical properties because of the tunability of their sizes (Huerta-Aguilar et al. 2019; Bhattacharya et al. 2020). At 500 nm, the LSPRs are more uniformly distributed. Regardless of working wavelength, all simulations presented an

**Fig. 7**  $|E|^2$  simulations of hexagonal and rounded vertexes of ZnO–NPs with different diameters embedded in DW performed at 300 nm and 360 nm of wavelength excitation. The bottom color scale is in V/m. The bar scale corresponds to 50 nm





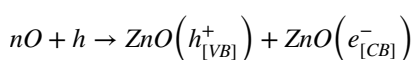
low band gap energy. Furthermore, the presence of surface oxygen vacancies is known to enhance the photocatalytic efficiency by improving the separation of the  $e^-/h^+$  pairs as well as increasing the adsorption of  $O_2$  on the ZnO nanocatalyst (Duraimurugan et al. 2019). Oxygen vacancies produce energy levels within the band gap of the ZnO nanoparticles. These levels serve as charge carrier traps that can capture the photogenerated charges and delay the recombination between the  $e^-/h^+$  pairs.

Green synthesized nanoparticles show better performance when compared to those synthesized using chemical/physical methods due to the bioactive compounds present in the plant extract which coat the surface of the photocatalyst, increasing its surface area, and providing a large number of surface area of the catalyst. It also increases the concentration of hydroxyl groups, and as a consequence, increases the production of reactive oxygen species (ROS) (Kumar and Dutta 2022) as described in the proposed degradation mechanism.

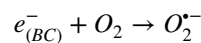
In a study published by Kuriakose et al. (2015), it was reported the photocatalytic activity of ZnO nanostructures and Cu doped with ZnO nanostructures for removing MB under sunlight irradiation conditions, observing an improvement in the MB removal with Cu–ZnO doped nanomaterial (92% of 10  $\mu$ M MB in 30 min) compared to pure ZnO. It was also demonstrated that the enhanced photocatalytic of Cu–ZnO nanostructures is attributed to the formation of nanoheterojunctions (ZnO–CuO) facilitating a better sunlight utilization efficiency. Liu et al. (2021) confirmed that the construction of heterojunction at the interface of two semiconductor photocatalysts plays a crucial role in separating and transporting charge carriers, contributing to a highly efficient photocatalytic reaction, reported to higher efficiencies in shorter time of light exposure.

As it is observed, pure ZnO NPs showed larger times for removing MB when compared to the results obtained in the previous studies, however, it is hypothesized that when a photocatalyst (ZnO NPs) is irradiated with photons with energies equal to or greater than the bandgap energy (3.18 eV), electrons ( $e^-$ ) are excited from the valence band (VB) to the conduction band (CB), simultaneously creating holes ( $h^+$ ) in vb.

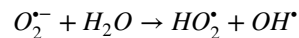
The photocatalytic mechanism of ZnO NPs is as follows (Legrini et al. 1993):



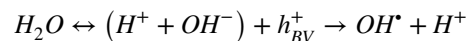
where  $h$  is the required electron transfer from the VB to CB. The electrons generated by irradiation are easily surrounded by  $O_2$  adsorbed on the surface of the catalyst to produce superoxide radicals ( $O_2^{\cdot-}$ ).



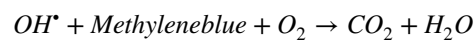
Subsequently, it can react with  $H_2O$  to produce the hydroperoxyl radical ( $HO_2^{\cdot}$ ) and hydroxyl radical ( $OH^{\cdot}$ ), which are strong oxidizing agents capable of decomposing organic molecules, such as MB.



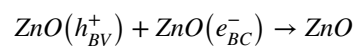
Simultaneously, the photoinduced holes are trapped by  $H_2O$  on the surface of the photocatalyst to produce hydroxyl radicals ( $OH^{\cdot}$ ).



Finally, the organic molecules are oxidized to produce carbon dioxide and water.



Meanwhile, the recombination of positive holes and electrons occurs, which reduces the photocatalytic activity of ZnO.



## Cell culture and cell viability assay

The rapid development of the application of ZnO nanoparticles in diverse fields such as medicine, cosmetics, food, and environmental remediation has led to the need for their safety as associated with human health. There is less certainty regarding nanoscale ZnO, even though bulk ZnO has been recognized as safe. Several studies have reported damage to eukaryotic cells, but there are no precise details regarding the cytotoxic mechanism or toxic concentration of NPs.

Multiple studies have reported the toxicity of nanoparticles when inhaled or ingested. To determine the effect of zinc nanoparticles on intestinal epithelial isolated from the large intestine (HCT 15) and purchases from American Type Culture Collection (ATCC). HCT 15 cells growing in RPMI cell culture medium were incubated with different nanoparticle concentrations for 24 h and the WST-1 cell viability assay was used to determine cell viability.

As shown in Fig. 10, zinc nanoparticle concentrations between 50 and 70  $\mu$ g/mL exhibited negligible toxicity in comparison to untreated control cells.

The toxicity of ZnO NPs produced through green synthesis and derived from various plant extracts has been the subject of many studies.

It is important to note that the toxicity of ZnO is specifically linked to its solubility, evident in the concentration of  $Zn^{2+}$ . In a study published by (Song et al. 2020) it was



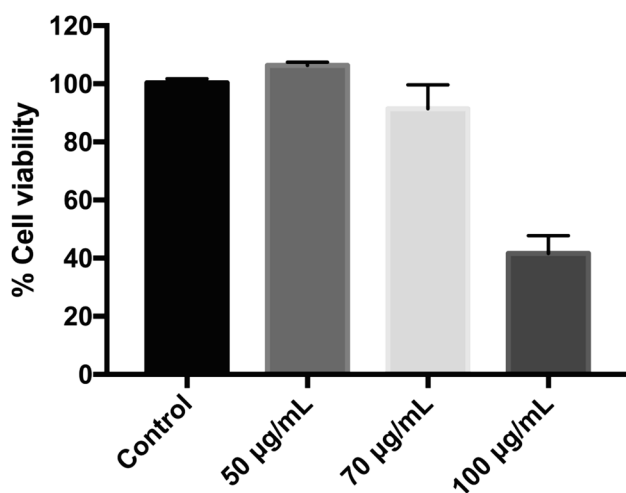


**Fig. 10** WST-1 viability for HCT 15 cells growth at different green synthesized ZnO NPs concentrations

reported that several factors such as exposure duration, culture conditions, and test mediums, can impact on the toxicity of ZnO nanoparticles NPs. In this study was evaluated the cytotoxicity of ZnO NPs, ZnO bulk particles (BPs), and  $Zn^{2+}$ , towards *E. coli*, observing that ZnO NPs and ZnO BPs had comparable cytotoxicity. The study revealed that the toxicity of ZnO NPs/BPs was decreased by  $Fe^{3+}$  in a concentration-dependent manner. The mechanisms of the decreased cytotoxicity of ZnO NPs were attributed to both decreased particle-related and ion-related toxicity, therefore, the presence of  $Fe^{3+}$  resulted in decreased cytotoxicity by the promotion of  $Zn^{2+}$ . The study concluded that the cytotoxicity of ZnO NPs can be partially attributed to Zn accumulation, which is governed by the solubility of ZnO. There are additional mechanisms of cytotoxicity including the produced by the reactive oxygen species (ROS), membrane disorganization, and DNA damage, which are also affected by the dynamic of ZnO and  $Zn^{2+}$  ratio in the medium. A remarkable statement of this previous work was that the cytotoxicity of ZnO NP was predominantly derived from particle-related toxicity (90%) after 8 h and after 24 h of exposure, the cytotoxicity was related to the presence of  $Zn^{2+}$  ions ( $\geq 80\%$ ).

As an important remark it is important to note that a complete understanding of the dissolution mechanism of ZnO NPs in the medium and most of the mechanisms leading to increasing intracellular  $[Zn^{2+}]$  levels remain speculative (Valdiglesias et al. 2023).

In a previous study published by Saravanan et al. (2018), it was hypothesized that free  $Zn^{2+}$  partially contributed an antimicrobial effect through the mechanical contact between the membrane of *Helicobacter pylori* and ZnO surface, interestingly, in the same experiment, the biosafety profile of the NPs was studied using normal human mesenchymal stem

cells (hMSc) with no significant toxicity to the mammalian cells at a concentration equal to and below 12.5 µg/ml.

Toxicity levels of metal oxide nanoparticles are also influenced by the kind of synthesis method used and the reaction conditions applied, which affect the surface atomic properties of the synthesized nanoparticles and their arrangements (Rana et al. 2020). For instance, Aswathi et al. (2023) reported that biodegradability and low toxicity are among the most significant characteristics of green-synthesized ZnO nanomaterials. In previous studies, (Mandal et al. 2018) proved that green synthesized ZnO NPs improved their photocatalytic activity and Hahm (2016) reported that ZnO nanoparticles showed acceptable biocompatibility to be used in detection modes in biological systems.

Our data indicate that cell viability was not affected by ZnO NPs at doses below 70 µg/mL. It is possible to postulate that the HTC 15 cells exhibited compatibility with the green synthesized ZnO NPs during culture. This improvement may be partially due to the residual organic molecules remaining from the *T. recurvata* extract after the synthesis process, which may have coated the nanoparticles to facilitate a less deleterious interaction with the cells. Furthermore, it is hypothesized that the cytotoxic effect of ZnO NPs is restricted to the initial hours of incubation, where the concentration of  $Zn^{2+}$  is low (Song et al. 2020).

It is worth noting that multiple studies have found ZnO NPs to be toxic to several cell systems and organisms. Nevertheless, most of these studies did not consider the potential interference of these nanoparticles with the components of the culture medium, reagents, or detection systems, which has been shown to be a critical factor in the observed results. This is why more research is needed to determine whether the toxicity of ZnO NPs is caused by the nanoparticles themselves or by the zinc ions that are released, as well as the cellular mechanisms.

In relation to the international regulation of Zn and Zn-based compounds in water, it is important to note that the permissible levels for these materials differ across different international regulations. For instance, the European Union has set a provisional recommendation value of 50 µg/L for total zinc in drinking water, which includes both soluble and insoluble forms of zinc but does not expressly address ZnO nanoparticles (98/83/EC 1998). Currently, there is no federal law or standard in the USA that specifies the maximum amount of ZnO nanoparticles that can be present in water, including both soluble and insoluble forms of zinc, and the Environmental Protection Agency (EPA) has set the maximum contamination level (MCL) for total zinc in drinking water at 5 mg/L. (USEPA 1979).

Finally, it is critical to understand that, in addition to the critical advances made in the fabrication and characterization of nanomaterials for environmental applications, a comprehensive assessment involving cytotoxic analysis is



required. This method may not only improve our comprehension of cell responses, but it may also help to uncover the potentially dangerous effects of nanoparticles release into the environment. As a result, for informed decision-making in environmental policies, a complete approach is necessary.

## Conclusion

For the first time, this study presents a feasible and environmentally friendly method for producing ZnO nanoparticles with strong photocatalytic activity and minimum toxicity effect on human epithelial cells, making them potentially useful in a variety of environmental applications. The green synthesis of ZnO nanoparticles using *T. recurvata* extracts is a viable strategy that can be expanded to manufacture a wide range of nanomaterials, providing an alternative to existing methods that frequently involve toxic chemicals and time-consuming processes. Overall, the findings of this work provide a green and sustainable approach for synthesizing ZnO nanoparticles with potential applications in a variety of industries. This study also includes results of the simulations of ZnO NPs varying shapes and sizes, as well as in individual or aggregated presentation; the use of these simulation tools significantly contributes to our understanding of the optical behavior of nanomaterials, enhancing our comprehension of the obtained photocatalytic response.

This new approach was useful for visualizing the plasmonic response of this semiconductor and elucidating the optical behavior of this nanoparticle, opening a broader range of applications for the same purposes.

**Supplementary Information** The online version contains supplementary material available at <https://doi.org/10.1007/s11356-024-31929-7>.

**Acknowledgements** E.V.-N. acknowledges the technical support provided by B.V.F. during the preparation of this manuscript. J. Álvarez-Martínez thanks the Consejo Nacional de Ciencia y Tecnología for his PhD Scholarship (CVU 886439).

### Authors' contributions

All the authors contributed to the conception and design of the study. Material preparation, data collection, and analysis were performed by Nayeli F. Ibarra-Cervantes, Edgar Vázquez-Núñez, Christian Gómez-Solis, Fabián Fernández-Luqueño, Gustavo Basurto-Islas, Jonathan Álvarez-Rodríguez, and Rigoberto Castro-Beltran. The first draft of the manuscript was written by Edgar Vázquez-Núñez, and all the authors commented on the previous versions of the manuscript. All authors have read and approved the final manuscript.

**Funding** This work was funded by DAIP, Universidad de Guanajuato through Convocatoria Institucional de Investigación Científica 2023, Grant number 034/2023 (E.V.-N). E.V.-N also was supported by DIQEB-DCI, Universidad de Guanajuato. R.C.-B. thanks the support of Dirección de Apoyo a la Investigación y al Posgrado (DAIP), Universidad de Guanajuato CIIC (035/2022 and 012/2023).

**Data availability** The data that support the findings of this study are available on request from the corresponding author.

## Declarations

**Ethics approval** This manuscript adheres to ethical guidelines by ensuring exclusive submission to one journal, maintaining originality with proper prior publication disclosure, and avoiding the practice of splitting up research. While we recognize justifiable circumstances for concurrent publication, this submission does not fall into that category. Our results are presented honestly without any data manipulation, and we have diligently avoided plagiarism by properly acknowledging external sources. We are dedicated to upholding the highest standards of research integrity throughout this submission process.

**Consent to participate** Not applicable.

**Consent for publication** Not applicable.

**Competing interests** The authors declare that they have no competing interests.

## References

- Abebe B, Murthy HA, Amare E (2020) Enhancing the photocatalytic efficiency of ZnO: defects, heterojunction, and optimization. *Environ Nanotechnol, Monitoring & Management* 14:100336
- Anbuvannan M, Ramesh M, Viruthagiri G et al (2015) Synthesis, characterization and photocatalytic activity of ZnO nanoparticles prepared by biological method. *Spectrochim Acta Part A Mol Biomol Spectrosc* 143:304–308
- Archer DG, Wang P (1990) The dielectric constant of water and Debye-Hückel limiting law slopes. *J Phys Chem Ref Data* 19:371–411
- Aswathi V, Meera S, Maria CA, Nidhin M (2023) Green synthesis of nanoparticles from biodegradable waste extracts and their applications: a critical review. *Nanotechnol Environ Eng* 8:377–397
- Bellotti N, Deyá C (2019) Natural products applied to antimicrobial coatings. *Stud Nat Prod Chem* 60:485–508
- Bhatia P, Nath M (2020) Green synthesis of p-NiO/n-ZnO nanocomposites: Excellent adsorbent for removal of congo red and efficient catalyst for reduction of 4-nitrophenol present in wastewater. *J Water Process Eng* 33:101017
- Bhattacharya D, Mukherjee S, Mitra RK, Ray SK (2020) Size-dependent optical properties of MoS<sub>2</sub> nanoparticles and their photocatalytic applications. *Nanotechnology* 31:145701
- Biswas A, Ahmed T, Rana MR et al (2023) Fabrication and characterization of ZnO nanoparticles-based biocomposite films prepared using carboxymethyl cellulose, Taro Mucilage, and Black Cumin Seed Oil for Evaluation of Antioxidant and Antimicrobial Activities. *Agronomy* 13:147
- Bitwell C, Sen IS, Luke C, Kakoma MK (2023) A review of modern and conventional extraction techniques and their applications for extracting phytochemicals from plants. *Sci Afr* 19:e01585
- Cai X, Liu X, Jiang J et al (2020) Molecular mechanisms, characterization methods, and utilities of nanoparticle biotransformation in nanosafety assessments. *Small* 16:1907663
- Chaudhari PL, Kale PC (2017) Synthesis and characterization of nano zinc peroxide photocatalyst for the removal of brilliant green dye from textile waste water. *Int J Chem Tech Res* 10:477–486
- Chemingui H, Moulahi A, Missaoui T et al (2022) A novel green preparation of zinc oxide nanoparticles with *Hibiscus sabdariffa* L.: photocatalytic performance, evaluation of antioxidant and antibacterial activity. *Environ Technol* 1–19
- Chen L, Batjikh I, Hurh J et al (2019) Green synthesis of zinc oxide nanoparticles from root extract of *Scutellaria baicalensis* and its

- photocatalytic degradation activity using methylene blue. *Optik* 184:324–329
- Council Directive 98/83/EC (1998) The quality of water intended for human consumption. available at <https://eur-lex.europa.eu/legal-content/EN/TXT/?uri=CELEX:31998L0083>
- Deak G, Dumitru F, Moncea M et al (2019) Synthesis of ZnO nanoparticles for water treatment applications. *Int J Conservation Sci* 10:343–350
- Dhiman V, Kondal N, Choudhary P (2023) Bryophyllum pinnatum leaf extract mediated ZnO nanoparticles with prodigious potential for solar driven photocatalytic degradation of industrial contaminants. *Environ Res* 216:114751
- Duraimurugan J, Kumar GS, Maadeswaran P et al (2019) Structural, optical and photocatalytic properties of zinc oxide nanoparticles obtained by simple plant extract mediated synthesis. *J Mater Sci: Mater Electron* 30:1927–1935
- Elmorsi TM, Elsayed MH, Bakr MF (2017) Enhancing the removal of methylene blue by modified ZnO nanoparticles: kinetics and equilibrium studies. *Can J Chem* 95:590–600
- Faisal S, Jan H, Shah SA et al (2021) Green synthesis of zinc oxide (ZnO) nanoparticles using aqueous fruit extracts of Myristica fragrans: their characterizations and biological and environmental applications. *ACS Omega* 6:9709–9722
- Fouda A, Eid AM, Abdelkareem A et al (2022) Phyco-synthesized zinc oxide nanoparticles using marine macroalgae, *Ulva fasciata* Delile, characterization, antibacterial activity, photocatalysis, and tanning wastewater treatment. *Catalysts* 12:756
- Gatou M-A, Lagopati N, Vagena I-A et al (2022) ZnO nanoparticles from different precursors and their photocatalytic potential for biomedical use. *Nanomaterials* 13:122
- Gherbi B, Laouini SE, Meneceur S et al (2022) Effect of pH value on the bandgap energy and particles size for biosynthesis of ZnO nanoparticles: Efficiency for photocatalytic adsorption of methyl orange. *Sustainability* 14:11300
- Goda H, Behrenbruch P (2004) Using a modified Brooks-Corey model to study oil-water relative permeability for diverse pore structures. SPE-88538-MS
- Gómez-Solís C, Juárez-Ramírez I, Moctezuma E, Torres-Martínez LM (2012) Photodegradation of indigo carmine and methylene blue dyes in aqueous solution by SiC–TiO<sub>2</sub> catalysts prepared by sol-gel. *J Hazard Mater* 217:194–199
- Gudkov SV, Burmistrov DE, Serov DA et al (2021) A mini review of antibacterial properties of ZnO nanoparticles. *Frontiers in Physics* 9:641481
- Hahn J (2016) Fundamental properties of one-dimensional zinc oxide nanomaterials and implementations in various detection modes of enhanced biosensing. *Annu Rev Phys Chem* 67:691–717
- Hamidian K, Sarani M, Barani M, Khakbaz F (2022) Cytotoxic performance of green synthesized Ag and Mg dual doped ZnO NPs using *Salvadora persica* extract against MDA-MB-231 and MCF-10 cells. *Arab J Chem* 15:103792
- Hassan SS, El Azab WI, Ali HR, Mansour MS (2015) Green synthesis and characterization of ZnO nanoparticles for photocatalytic degradation of anthracene. *Adv Natural Sci: Nanosci Nanotechnol* 6:045012
- Hermans T, Nguyen F, Robert T, Revil A (2014) Geophysical methods for monitoring temperature changes in shallow low enthalpy geothermal systems. *Energies* 7:5083–5118
- Huerta-Aguilar CA, Ramírez-Alejandre AA, Thangarasu P et al (2019) Crystal phase induced band gap energy enhancing the photocatalytic properties of Zn–Fe<sub>2</sub>O<sub>4</sub>/Au NPs: experimental and theoretical studies. *Catal Sci Technol* 9:3066–3080
- Ibañez JG, Solorza O, Gomez-del-Campo E (1991) Preparation of semiconducting materials in the laboratory: production of CdS thin films and estimation of their band gap energy. *J Chem Educ* 68:872
- Islam F, Shohag S, Uddin MJ et al (2022) Exploring the journey of zinc oxide nanoparticles (ZnO-NPs) toward biomedical applications. *Materials* 15:2160
- Jamkhande PG, Ghule NW, Bamer AH, Kalaskar MG (2019) Metal nanoparticles synthesis: An overview on methods of preparation, advantages and disadvantages, and applications. *J Drug Delivery Sci Technol* 53:101174
- Jayaraj SK, Sadishkumar V, Arun T, Thangadurai P (2018) Enhanced photocatalytic activity of V<sub>2</sub>O<sub>5</sub> nanorods for the photodegradation of organic dyes: a detailed understanding of the mechanism and their antibacterial activity. *Mater Sci Semicond Process* 85:122–133
- Jigna P, Sumitra C (2008) Phytochemical screening of some plants from western region of India. *Plant Archives* 8:657–662
- Kabir MH, Ali MM, Kaiyum MA, Rahman M (2019) Effect of annealing temperature on structural morphological and optical properties of spray pyrolyzed Al-doped ZnO thin films. *J Physics Comm* 3:105007
- Kamarulzaman N, Kasim MF, Rusdi R (2015) Band gap narrowing and widening of ZnO nanostructures and doped materials. *Nanoscale Res Lett* 10:1–12
- Khan N, Kalam MA, Alam MT et al (2023) Drug standardization through pharmacognostic approaches and estimation of anticancer potential of chamomile (*Matricaria chamomilla* L.) using prostate-cancer cell lines: an in-vitro study. *J Cancer* 14:490–504
- Khan SA, Khan SB, Khan LU et al (2018) Fourier transform infrared spectroscopy: fundamentals and application in functional groups and nanomaterials characterization. *Handbook of materials characterization* 317–344
- Kilpeläinen P, Liski E, Saranpää P (2023) Optimising and scaling up hot water extraction of tannins from Norway spruce and Scots pine bark. *Ind Crops Prod* 192:116089
- Kirana SY, Febrianti R, Amananti W (2023) Determination of total flavonoid content of *Bajakah* Tampala and *Kalalawit* roots using the reflux. *Indonesian J Chem Sci Technol (IJCST)* 6:56–64
- Krishnan A, Swarnalal A, Das D et al (2023) A review on transition metal oxides based photocatalysts for degradation of synthetic organic pollutants. *J Environ Sci* 139:389–417
- Kumar G, Dutta RK (2022) Sunlight-induced enhanced photocatalytic reduction of chromium (VI) and photocatalytic degradation of methylene blue dye and ciprofloxacin antibiotic by Sn<sub>3</sub>O<sub>4</sub>/SnS<sub>2</sub> nanocomposite. *Environ Sci Pollut Res* 29:57758–57772
- Kumar MA, Ravikumar C, Nagaswarupa H et al (2019) Evaluation of bi-functional applications of ZnO nanoparticles prepared by green and chemical methods. *J Environ Chem Eng* 7:103468
- Kumbhar D, Kumbhar S, Salunke G et al (2019) Effect of Cu doping on structural and optical properties of ZnO nanoparticles using sol-gel method. *Macromol Symp* 387:1800192
- Kuriakose S, Satpati B, Mohapatra S (2015) Highly efficient photocatalytic degradation of organic dyes by Cu doped ZnO nanostructures. *Phys Chem Chem Phys* 17:25172–25181
- Lal S, Verma R, Chauhan A et al (2022) Antioxidant, antimicrobial, and photocatalytic activity of green synthesized ZnO-NPs from *Myrica esculenta* fruits extract. *Inorg Chem Commun* 141:109518
- Lasso P, Rojas L, Arévalo C et al (2022) *Tillandsia usneoides* extract decreases the primary tumor in a murine breast cancer model but not in melanoma. *Cancers* 14:5383
- Legrini O, Oliveros E, Braun A (1993) Photochemical processes for water treatment. *Chem Rev* 93:671–698
- Li N, Xu G, Yan M et al (2023) Fabrication of vertically aligned ZnO nanorods modified with dense silver nanoparticles as effective sensors substrates. *Chemosensors* 11:210
- Limpachanangkul P, Jedsukontorn T, Zhang G et al (2019) Comparative photocatalytic behavior of photocatalysts (TiO<sub>2</sub>, SiC, Bi<sub>2</sub>O<sub>3</sub>, ZnO) for transformation of glycerol to value added compounds. *Korean J Chem Eng* 36:1527–1535

- Liu B, Bie C, Zhang Y et al (2021) Hierarchically porous ZnO/g-C<sub>3</sub>N<sub>4</sub> S-scheme heterojunction photocatalyst for efficient H<sub>2</sub>O<sub>2</sub> production. *Langmuir* 37:14114–14124
- Lo M-M, Benfodda Z, Dunyach-Rémy C et al (2022) Isolation and identification of flavones responsible for the antibacterial activities of *Tillandsia bergeri* extracts. *ACS Omega* 7:35851–35862
- Luna-Cozar J, Martínez-Madero O, Jones RW (2020) Ball Moss, *Tillandsia recurvata* L., as a refuge site for arthropods in a seasonally dry tropical forest of Central Mexico. *Southwestern Entomologist* 45:445–460
- Mandal T, Malhotra S, Singha R (2018) Photocatalytic degradation of methylene blue in presence of ZnO nanopowders synthesized through a green synthesis method. *Rev Rom Mater* 48:32–38
- Marica I, Nekvapil F, Ștefan M et al (2022) Zinc oxide nanostructures for fluorescence and Raman signal enhancement: a review. *Beilstein J Nanotechnol* 13:472–490
- Matinise N, Fuku X, Kaviyarasu K et al (2017) ZnO nanoparticles via *Moringa oleifera* green synthesis: Physical properties & mechanism of formation. *Appl Surf Sci* 406:339–347
- Merakeb MS, Brihi N, Ferhat R, Yanat B (2023) Inhibitory effects of *linum usitatissimum* alkaloid on inflammatory and nociceptive responses in mice. *Curr Bioact Compd* 19:56–62
- Mirzaei H, Darroudi M (2017) Zinc oxide nanoparticles: Biological synthesis and biomedical applications. *Ceram Int* 43:907–914
- Modi S, Fulekar M (2020) Green synthesis of zinc oxide nanoparticles using garlic skin extract and its characterization. *J Nanostructures* 10:20–27
- Mumanga TJ, Díaz-Torres LA, Gómez-Solís C (2021) Nd<sup>3+</sup> doped BaAl<sub>2</sub>O<sub>4</sub> for enhanced photocatalytic degradation of methylene blue. *Mater Lett* 292:129664
- Muthuvel A, Jothibas M, Manoharan C (2020) Effect of chemically synthesis compared to biosynthesized ZnO-NPs using *Solanum nigrum* leaf extract and their photocatalytic, antibacterial and in-vitro antioxidant activity. *J Environ Chem Eng* 8:103705
- Nagamalleswari T, Modem Sreenivasulu (2023) Multifunctional properties of gadolinium doped annealed zinc oxide nanoparticles. *Phys Scripta* 98:035812
- Nang An V, Van TT, Nhan HT, Van Hieu L (2020) Investigating methylene blue adsorption and photocatalytic activity of ZnO/CNC nanohybrids. *J Nanomater* 2020:1–10
- Nguyen VN, Tran DT, Nguyen MT et al (2018) Enhanced photocatalytic degradation of methyl orange using ZnO/graphene oxide nanocomposites. *Res Chem Intermed* 44:3081–3095
- Nguyen DTC, Le HT, Nguyen TT et al (2021) Multifunctional ZnO nanoparticles bio-fabricated from *Canna indica* L flowers for seed germination, adsorption, and photocatalytic degradation of organic dyes. *J Hazardous Mat* 420:126586
- Nouri-Mashiran M, Taghavi L, Fataei E et al (2022) Green synthesis of ZnO nanoparticles and comparison of 2, 4-dinitrophenol removal efficiency using photocatalytic, sonocatalytic, and adsorption processes. *Main Group Chem* 21:559–575
- Obayomi KS, Oluwadiya AE, Lau SY et al (2021) Biosynthesis of *Tithonia diversifolia* leaf mediated zinc oxide nanoparticles loaded with flamboyant pods (*Delonix regia*) for the treatment of methylene blue wastewater. *Arab J Chem* 14:103363
- Omar FS, Nay Ming H, Hafiz SM, Ngee LH (2014) Microwave synthesis of zinc oxide/reduced graphene oxide hybrid for adsorption-photocatalysis application. *International Journal of Photoenergy* 2014:
- Osuntokun J, Onwudiwe DC, Ebenso EE (2019) Green synthesis of ZnO nanoparticles using aqueous *Brassica oleracea* L. var. *italica* and the photocatalytic activity. *Green Chem Lett Rev* 12:444–457
- Parashar M, Shukla VK, Singh R (2020) Metal oxides nanoparticles via sol–gel method: a review on synthesis, characterization and applications. *J Mater Sci: Mater Electron* 31:3729–3749
- Pérez-López M, Flores-Cruz M, Martínez-Vázquez M et al (2020) Anti-virulence activities of some *Tillandsia* species (Bromeliaceae). *Botanical Sciences* 98:117–127
- Purewal SS, Verma P, Kaur P, et al (2023) A comparative study on proximate composition, mineral profile, bioactive compounds and antioxidant properties in diverse carrot (*Daucus carota* L.) flour. *Biocatalysis and Agricultural Biotechnology*. 48:102640
- Rana A, Yadav K, Jagadevan S (2020) A comprehensive review on green synthesis of nature-inspired metal nanoparticles: Mechanism, application and toxicity. *J Clean Prod* 272:122880
- Renda C, Goulart L, Fernandes C et al (2021) Novel onion-like carbon structures modified with iron oxide as photocatalysts for the degradation of persistent pollutants. *J Environ Chem Eng* 9:104934
- Sadiq H, Sher F, Sehar S et al (2021) Green synthesis of ZnO nanoparticles from *Syzygium Cumini* leaves extract with robust photocatalysis applications. *J Mol Liq* 335:116567
- Salem SS, Fouda A (2021) Green synthesis of metallic nanoparticles and their prospective biotechnological applications: an overview. *Biol Trace Elem Res* 199:344–370
- SAS Institute (1989) *Statistic guide for personal computers*
- Sasi S, Fasma PF, Sharmila TB et al (2022) Green synthesis of ZnO nanoparticles with enhanced photocatalytic and antibacterial activity. *J Alloy Compd* 924:166431
- Shah A, Haq S, Rehman W et al (2019) Photocatalytic and antibacterial activities of paeonia emodi mediated silver oxide nanoparticles. *Materials Research Express* 6:045045
- Sharma I, Sharma P, Hassanien AS (2022) Optical properties and optoelectrical parameters of the quaternary chalcogenide amorphous Ge<sub>15</sub>S<sub>n</sub>S<sub>35-x</sub>Te<sub>50</sub> films. *J Non-Cryst Solids* 590:121673
- Song K, Zhang W, Sun C et al (2020) Dynamic cytotoxicity of ZnO nanoparticles and bulk particles to *Escherichia coli*: a view from unfixed ZnO particle: Zn<sup>2+</sup> ratio. *Aquat Toxicol* 220:105407
- Tan S, Li Q, Guo L et al (2023) Investigation of foaming behavior in herbal extracts via the characterization of solution environment for reverse osmosis concentration. *Food Bioprod Process* 137:28–44
- Tauc J, Menth A (1972) States in the gap. *J Non-Cryst Solids* 8:569–585
- Thamer FH, Thamer N, Alhamzi A et al (2023) Antioxidant capacity, total phenol contents and phytochemical screening of *Citrullus colocynthis* crust, pulp and seeds extracts. *Am J Biochem Biotechnol* 19:12–19
- Thi TUD, Nguyen TT, Thi YD et al (2020) Green synthesis of ZnO nanoparticles using orange fruit peel extract for antibacterial activities. *RSC Adv* 10:23899–23907
- Tolossa WK, Shibeshi PT (2022) Structural, optical and enhanced antibacterial activities of ZnO and (Co, Fe) co-doped ZnO nanoparticles by sol-gel combustion method. *Chem Phys Lett* 795:139519
- Tosi G, Duskey J, Kreuter J (2020) Nanoparticles as carriers for drug delivery of macromolecules across the blood-brain barrier. *Expert Opin Drug Deliv* 17:23–32
- Turan NB, Erkan HS, Engin GO, Bilgili MS (2019) Nanoparticles in the aquatic environment: Usage, properties, transformation and toxicity—a review. *Process Saf Environ Prot* 130:238–249
- United States Environmental Protection Agency (1979) *National Secondary Drinking Water Regulations EPA 570/9-76-000*; US EPA, Washington, DC, p 39
- Uribe-López M, Hidalgo-López M, López-González R et al (2021) Photocatalytic activity of ZnO nanoparticles and the role of the synthesis method on their physical and chemical properties. *J Photochem Photobiol, A* 404:112866
- Valdiglesias V, Alba-González A, Fernández-Bertólez N et al (2023) Effects of zinc oxide nanoparticle exposure on human glial cells and zebrafish embryos. *Int J Mol Sci* 24:12297
- Vasiljevic Z, Dojcinovic M, Vujanecvic J et al (2020) Photocatalytic degradation of methylene blue under natural sunlight using iron

- titanate nanoparticles prepared by a modified sol–gel method. *Royal Soc Open Sci* 7:200708
- Verma R, Pathak S, Srivastava AK et al (2021) ZnO nanomaterials: green synthesis, toxicity evaluation and new insights in biomedical applications. *J Alloy Compd* 876:160175
- Yusof NAA, Zain NM, Pauzi N (2019) Synthesis of ZnO nanoparticles with chitosan as stabilizing agent and their antibacterial properties against Gram-positive and Gram-negative bacteria. *Int J Biol Macromol* 124:1132–1136
- Zapata-Campos CC, García-Martínez JE, Chavira JS et al (2020) Chemical composition and nutritional value of leaves and pods of *Leucaena leucocephala*, *Prosopis laevigata* and *Acacia farnesiana* in a xerophilous shrubland. *Emir J Food Agr* 32:723–730

**Publisher's Note** Springer Nature remains neutral with regard to jurisdictional claims in published maps and institutional affiliations.

Springer Nature or its licensor (e.g. a society or other partner) holds exclusive rights to this article under a publishing agreement with the author(s) or other rightsholder(s); author self-archiving of the accepted manuscript version of this article is solely governed by the terms of such publishing agreement and applicable law.